JOURNAL OF SOLID STATE CHEMISTRY 66, 125–135 (1987)

Domain Formation and Interfaces in Praseodymium and Terbium Oxides Obtained by Reduction of PrO_2 and TbO_2: A Comparison with Group Theory Predictions

C. BOULESTEIX* AND L. EYRING†

Department of Chemistry and Center for Solid State Science, Arizona State University, Tempe, Arizona 85287

Received February 24, 1986

The reduction of PrO_2 and TbO_2 may occur during their study by electron microscopy with the formation of ordered intermediate phases which can be considered as superstructures of a common prototype structure: the fluorite-type with unordered oxygen vacancies. Indeed, the different oxides that may occur are directly or indirectly obtained by reduction of fluorite-type PrO_2 and TbO_2 crystals. Reduction frequently ends with Pr_7O_{12} or Tb_7O_{12} (iota structure) to which special attention has been devoted here. Eight orientation variants of iota could occur within a unique fluorite prototype. Generally, only two of them are observed together. This has been attributed to a possible thin layer effect. Seven glide domains may also be present in the same iota orientation variant resulting from reduction of the fluorite prototype structure. Such glide domains are usually observed in Pr_7O_{12} and sometimes in Tb_7O_{12}. Layers occurring between glide domains have been identified as regions of different composition. Twelve different orientation variants can occur within the zeta (Pr_9O_{16}) or delta ($Tb_{11}O_{20}$) structures; two of them are frequently observed together. Different kinds of interfaces can be observed between different kinds of domains. For example, interfaces are generally irregular between different iota variants but are perfectly planar between iota and zeta phases. It is shown that the latter case must result from the formation of strain-free (low energy) interfaces.

Introduction

Electron beam induced reactions occur when PrO_2 or TbO_2 are imaged in the high-vacuum column of a high-resolution electron microscope (HREM) (*1*, *2*). Frequently in these studies, the reduction was terminated with the formation of the iota phase (Pr_7O_{12} or Tb_7O_{12}), but the phi phase, the cubic form of the sesquioxides, is observed if the processes are continued. It must be noted that the paths of reduction for PrO_2 and TbO_2 are different. In PrO_x reduction probably occurs sequentially through various intermediate states including the zeta (Pr_9O_{16}) or the epsilon ($Pr_{10}O_{18}$) structures while in TbO_x it occurs through the formation of the beta or delta intermediate states ($Tb_{12}O_{22}$ or $Tb_{11}O_{20}$). However, other compounds sometimes appear through the reduction process. For example, two different kinds of $Tb_{12}O_{22}$ can be encountered. Reduction beyond the phi phase (R_2O_3) is not achieved in the microscope. However, it has been shown that Pr_2O_3 can be transformed to the hexagonal structure by strong beam heating inside the electron microscope, and the monoclinic

* On leave from the University of Aix-Marseille III (CNRS-U.A 797) France.

† To whom inquiries should be addressed.

0022-4596/87 $3.00

structure can also be seen by quenching from high temperatures. Tb_2O_3 recrystallizes giving large cubic crystals under the same conditions (*3, 4*).

The reduction of PrO_x and TbO_x effected by the electron beam in the normal conditions of electron microscopic study frequently stops at the iota stage. Hence, the formation of the iota phase will be the focus of our attention. The structure of the iota phase has been determined. Iota, considered as a superstructure of fluorite, occurs with both orientation variants and glide domains. Some of each have been observed to occur in the same sample. Here, we will first explain why lower-oxide structures can be treated as superstructures of a fluorite prototype and what can be concluded from this. We will then compare these theoretical predictions with experimental results and show the existence of orientation variants and glide domains as expected from theoretical considerations. The mechanism of the formation of the iota phase through epsilon, zeta, or delta phases will be considered. A very striking point is the formation of one-directional interfaces between iota, zeta, and delta phases. This can be related to the formation of strain-free interfaces. By contrast, different orientation variants of the iota structure give rather irregular interfaces. Different stacking faults visible in the iota regions can be related to the reduction mechanism. They have been shown to be slices of a different composition.

A Group Theory Approach to Domain Formation in the Reduction of the Higher Pr and Tb Oxides

All the intermediate oxides below RO_2 except the hexagonal and monoclinic structures of R_2O_3 can be described as fluorite crystals where vacancies (here considered a special kind of atom) replace some oxygen atoms. The unordered structures which exist at high temperature for a large range of composition are cubic of the fluorite type. All of the low-temperature structures can be treated as ordered structures coming from the same fluorite prototype structure (except for a small deformation of the lattice that will not be taken into account here). The group theory for ordering is then valid and it can be used in the very simple way used by Van Tendeloo and Amelinckx (*5*). Let us consider first the case of iota. Zeta and delta will be considered thereafter.

1. Orientation variants of iota. PrO_2 and TbO_2 are of the fluorite structure of the $m3m$ point group of order 48, while iota is of the $\bar{3}$ point group of order 6. There are then n = 48/6 = 8 different orientation variants of the iota structure obtainable from the reduction of a fluorite-type crystal.

The reduction from the fluorite structure to iota occurs such that the threefold axis of iota is parallel to a $\langle 111\rangle_F$ direction (index F refers to the fluorite structure) and the **a**, **b**, **c** directions of iota are parallel to the $\langle 211\rangle_F$ directions. Twelve different $\langle 211\rangle_F$ axes occur and each axis of a variant is parallel to three $\langle 211\rangle_F$ axes so that each $\langle 211\rangle_F$ axis is parallel to $n = 8\times3/12 = 2$ axis of two different variants (Fig. 1). Domains of iota are related by the missing symmetries of the fluorite structure. In this case the missing symmetry operations make a variant

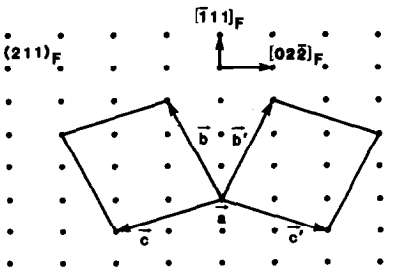

FIG. 1. A projection of the unit cells of the two iota (R_7O_{12}) variants onto the $(211)_F$ plane parallel to the $[211]_F$ axis. The $\langle 100\rangle_t$ axis is parallel to the $[211]_F$ direction. These two variants are related by a $(01\bar{1})$ plane of symmetry perpendicular to $[211]_F$ and containing the $[\bar{1}11]$ direction.

generating group (VGG): $4mm$. For example, $4mm$ is a subgroup of $m3m$ of order 8 without a common element with $\bar{3}$ (except for the identity), and the product of the order of $\bar{3}$ (6) by the order of $4mm$ (8) is equal to the order of $m3m$ (48) so that $4mm$ is a possible VGG for the different orientation variants of iota. This VGG is made of the following elements $[E]$, $[C_4^2]$, $[C_4^1, C_4^3]$, $[m_1, m_2]$, $[m_1', m_2']$ where the elements have been indicated by class, and where m_1 and m_2 represent symmetry operations about $\{100\}_F$ planes and m_1' and m_2' about $\{110\}_F$ planes. It must be noticed that the two variants named ι and ι' corresponding to the same $[211]_F$ axis are related (see Fig. 1) by symmetry operations about the $(01\bar{1})_F$ plane. They are then related by an m' operation. Each of them is related to the six others by the six other symmetry operations (except for the identity). Let us notice that 422 and $\bar{4}2m$ of order 8 would also have been possible VGG's (but not $4/m$ because of the inversion). When looking along a $[211]_F$ axis for the two orientation variants (ι and ι'), the electron beam is parallel to an **a** or **b** or **c** axis of iota. These two variants will be imaged in a similar way, but the other variants will be imaged differently. This point will be treated later.

2. Orientation variants of zeta or delta. Zeta occurs in Pr oxides (Pr_9O_{16}), delta in Tb oxides ($Tb_{11}O_{20}$), but since they have the same point group, $\bar{1}$, the same general mathematical treatment applies to both. Fluorite being $m3m$ (order 48) and zeta or delta $\bar{1}$ (order 2) the number of equivalent orientation variants is n = 48/2 = 24. The $\bar{4}3m$ is the only possible VGG in this case.

Epitaxial growth occurs such that **a** and **c** are both parallel to $\langle 211\rangle_F$ axes so that each of the twelve $\langle 211\rangle_F$ axes is parallel to $n = 24\times2/12 = 4$ edges (**a** or **c**) of delta or zeta phases of different orientation variants (Fig. 2). All the orientation variants have the same probability of being initiated in the

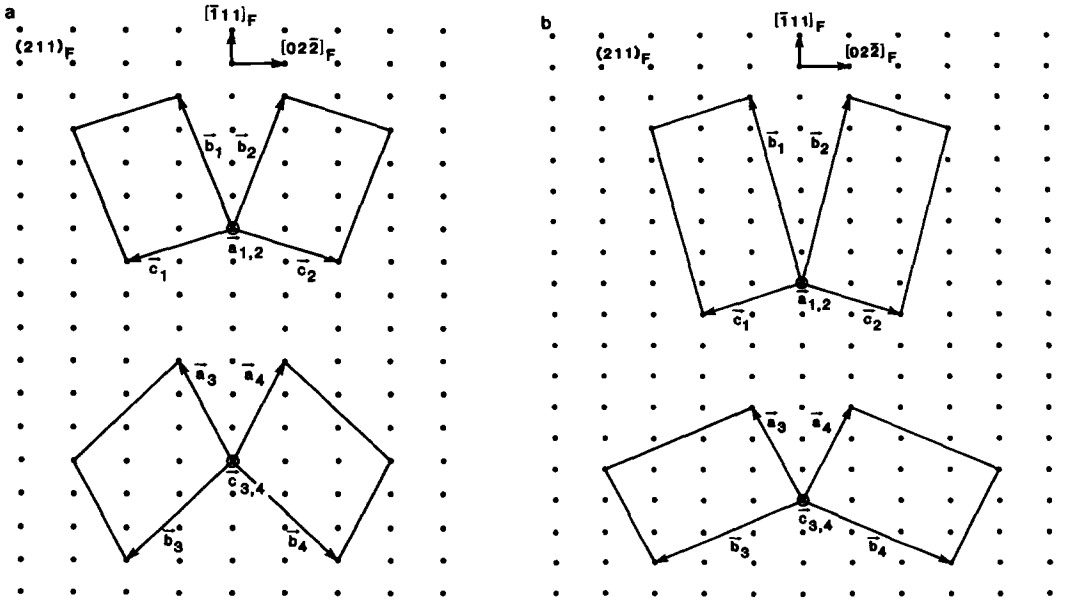

FIG. 2. (a) A projection parallel to the $[211]_F$ axis, onto the $(211)_F$ plane, of the unit cells of the four zeta (R_9O_{16}) variants that have an axis (**a** or **c**) parallel to the $[211]_F$ direction. (b) A projection parallel to the $[211]_F$ axis, onto the (211) plane, of the unit cells of the four delta ($R_{11}O_{20}$) variants that have an axis (**a** or **c**) parallel to the [211] direction.

bulk material. The four different variants that have an axis (**a** or **c**) parallel to one $[211]_F$ axis are indicated in Fig. 2; they are different for zeta (Fig. 2a) and delta (Fig. 2b). The image of these four different orientation variants will have a superstructure and the others will not, as will be seen later.

3. Glide domains for iota, zeta, and delta. The ratios of the volumes of the unit cells of iota, zeta, and delta, which are primitive, to the volume of the unit cell of the fluorite prototype, which is face centered cubic, are 7/4, 9/4, and 11/4 so that the relative ratios of the volumes of primitive unit cells are, respectively, 7, 9, and 11 and as many glide domains can occur in each case.

Experimental Results and Discussion

The iota structure is relatively stable under the conditions inside the electron microscope so that many experimental results have been obtained for this structure. Among these results are many showing the domain structure (orientation variants and glide domains) formed by the reduction of zeta (for Pr) or of delta (for Tb). Three aspects will be reported independently, first the existence of orientation variants, then glide domains, and finally the formation of the structure itself by reduction.

1. The Domain Structure of Iota: Orientation Variants

At high temperatures a cubic structure exists of the fluorite form with unordered vacancies (*6*). This structure exists over a rather large range of compositions. The formation of iota from this unordered structure, which is the prototype of the structures studied here, should be given by the theoretical model already developed. However, agreement with theoretical predictions suggests that iota is obtained by reduction of PrO_2 through zeta (Pr_9O_{16}) or through epsilon ($Pr_{10}O_{18}$), or similarly for terbia, by reduction of TbO_2 through delta ($Tb_{11}O_{20}$).

Different orientation variants are frequently observed in the same region, the most characteristic domain structure being obtained by reduction of epsilon (Fig. 3) where a great number of small domains of two different orientation variants (ι and ι') of iota are visible. The same variants (regions A and B) are also seen in iota obtained by reduction of zeta (Fig. 4a). Notice in region A of this figure the great number of planar defects that will be related later to glide domains. In each case (Figs. 3 and 4) the lattice image is obtained when the electron beam is parallel to one of the ⟨100⟩ axes of iota. As previously shown, two different orientation variants (ι and ι') have one ⟨100⟩ axis in common. A diffraction pattern of these two variants is given (Fig. 4b). The main spots are related to the fluorite structure while the others are related to the vacancy ordering in iota. For all of the other six orientation variants only the substructure spots would appear in the diffraction pattern; hence, as for the fluorite structure itself (which is unresolved under the conditions used here), no lattice image would be visible for these other six variants. This situation occurs in Fig. 4a suggesting that the region C, without lattice images, can reasonably be considered as an iota orientation variant which is not ι or ι'. It must be noticed that (Fig. 4a) an overlapping of the variant without superstructure with ι' exists between B and C. This would not be unexpected since ι and ι' are observed to overlap. Regions without a lattice image are, however, rarely observed in these thin crystals. Lattice images have usually been taken along the [001] iota axis, which means that their surfaces are close to the (001) iota plane. In nearly every instance only ι and ι' variants are present together. This could be related to an orientation of the surface that would induce some special orientation of iota as to reduce the surface

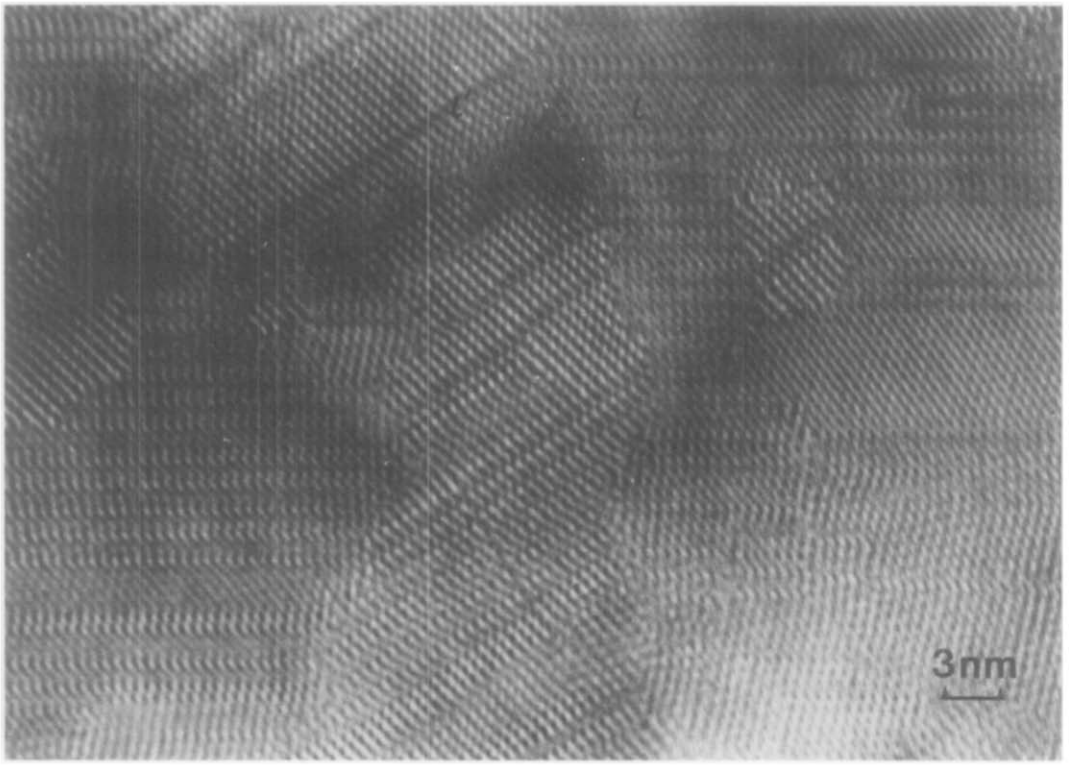

FIG. 3. An electron micrograph showing an intergrowth of two orientation variants (ι and ι') of Pr_7O_{12} (iota) obtained in reduction through $Pr_{10}O_{18}$ (epsilon). Glide domains separated by stacking faults are also apparent in each orientation variant.

energy. In this event, we would be dealing with some thin-layer effect.

Irregular interfaces occur between ι and ι', hence overlapping of these two structures is expected to sometimes occur parallel to the surface. The overlapping of ι and ι' is so prevalent (Fig. 5a) that it will be used later for the study of the glide. The orientation of interfaces could easily change under the operating conditions inside the electron microscope but they are, in fact, very stable and do not easily reorient so as to be perpendicular to surfaces. Interfaces between ι and ι' can then be considered to be very low-energy interfaces. The strain energy is especially low for such interfaces. This is to be expected if we consider the twin as a twin by a difference in the vacancy ordering in a fluorite structure without any change of size. Such an interface can be considered as being strain free, which is the source of a low surface energy. There is, however, a small deformation of the structure which accompanies the vacancy ordering (this amounts to a change of about 0.3 ° in the value of α in the iota structure from 99.6°, the expected value without deformation, to 99.28°) so that some strain energy could occur at the interface. The small value of the strain energy deduced from the nature of the interfaces can be attributed to the small extent of the deformation.

2. Glide Domains and the Use of Overlapping Regions for Their Study

Following the reduction to the iota structure a high density of planar defects is visi-

ble in each of the orientation variants. These defects are generally parallel to only one [100] direction of iota. This will be linked later to the path of formation of iota by reduction of zeta or delta. Figure 5a is an enlargement of a region neighboring that of Fig. 4a where the two orientation variants ι and ι' overlap. A rectangular pattern of white spots is visible with displacements in the overlapping region as marked by black rectangles. Figure 5b is a schematic drawing of the position of the white spots and of how the pattern is shifted in regions where stacking faults of ι go through the overlapping region. Figure 5c shows how these white dots occur by superposition of the two lattices of ι and ι' in projection along the common [100] direction (this is confirmed by image computation). A common superlattice shown schematically in Fig. 5c is formed in projection. A shift in position of the origin of the ι structure from position 0 to 1, 2, 3, 4, 5, 6 makes, respectively, a shift in position of the common superlattice position from position 0 to 6, 1, 5, 3, 4, 2 so that is appears as an enlargement of the shift in position of the ι structure on either side of a defect. This situation occurs along the faulted region I of iota. The shift in position of the common superlattice can be related to the only defect I of ι. This stacking fault can easily be correlated to a shift of the common superlattice from 0 to 1 (Fig. 5b) so that it corresponds to a glide of ι from 0

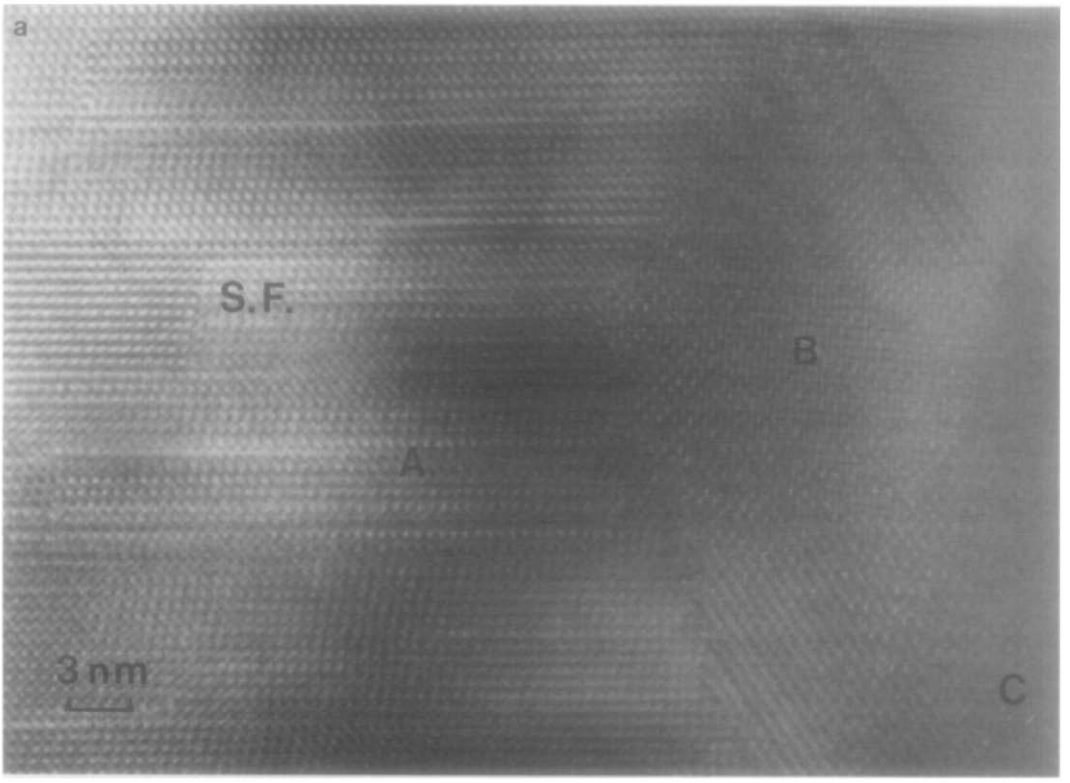

FIG. 4. (a) An electron micrograph showing two orientation variants (ι and ι') of Pr_7O_{12} (iota) obtained through Pr_9O_{16} (zeta) occurring together (A and B regions). In the C region the superstructure is very weak and could be due to an overlap of an orientational variant of iota that has no superstructure with ι'. In region A the one-directional stacking faults are very prominent. A stacking fault in another direction is marked S.F. (b) A diffraction pattern of a region including that of (4a).

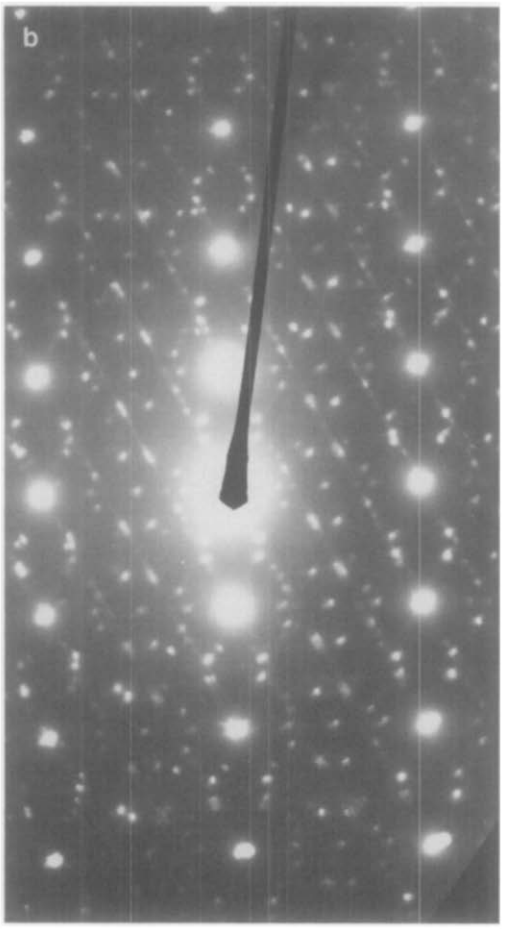

FIG. 4—*Continued.*

to 2. This is in agreement with direct observation of the high-resolution image on each side of the defect. A shift of about $\frac{1}{2}$ of a lattice distance exists on each side of the fault. This region contains two faults separated by a narrow band of good crystal. A careful study of the overlapping region shows that the dissociation of this stacking fault still exists inside the overlapping region and that each fault corresponds to a glide from 0 to 1 for the position of the white dots. Each defect, corresponding for ι to a glide from 0 to 1, gives on the image a small glide in agreement with the direct observation of the lattice image (in agreement also with previous results because two glides from 0 to 6 are equivalent to one glide from 0 to 2). Each defect can now be analyzed because the glide vector is known to be the same for each of them. Figure 5d is a representation of stacking faults IA and IB. The faults extend for one unit cell so that it is possible to identify the composition of the oxide inside this unit cell as Pr_8O_{14}. The slab of iota between the faults consists of three unit cells. The same result is obtained from the direct observation of the lattice image. Fault II is more complicated because a defect of ι' also occurs in the overlapping region. A very careful measurement of the shift of the white dots fits only with a shift of ι' corresponding to one defect of Pr_8O_{14} composition and two defects of ι of the same composition. The great similarity in the image of defects I and II confirms this point of view.

3. Formation of Iota from Epsilon or Zeta (for Pr) and from Delta (for Tb)

From epsilon. In all cases the formation of iota occurs by a loss of oxygen atoms and by vacancy ordering. The oxygen atoms are very mobile in these structures (*7*). Though epsilon is monoclinic, the pseudocubic cell is nearly such that $a = b = c = 5.482$ with the angles very close to 90° so that, for our purposes, a cubic symmetry exists in epsilon (except for vacancy positions). The deformation from the cubic structure is also small for iota as seen previously except for vacancy ordering. It is expected then that the transition from epsilon to iota would give domains as expected in the transition from unordered prototype to ordered structure. Different domains of different orientation are indeed obtained (Fig. 3) and numerous stacking faults are visible corresponding to glide domains. The shape of domains is irregular but their sizes are of the same order in different directions. They have probably developed from a great number of nuclei growing in different directions

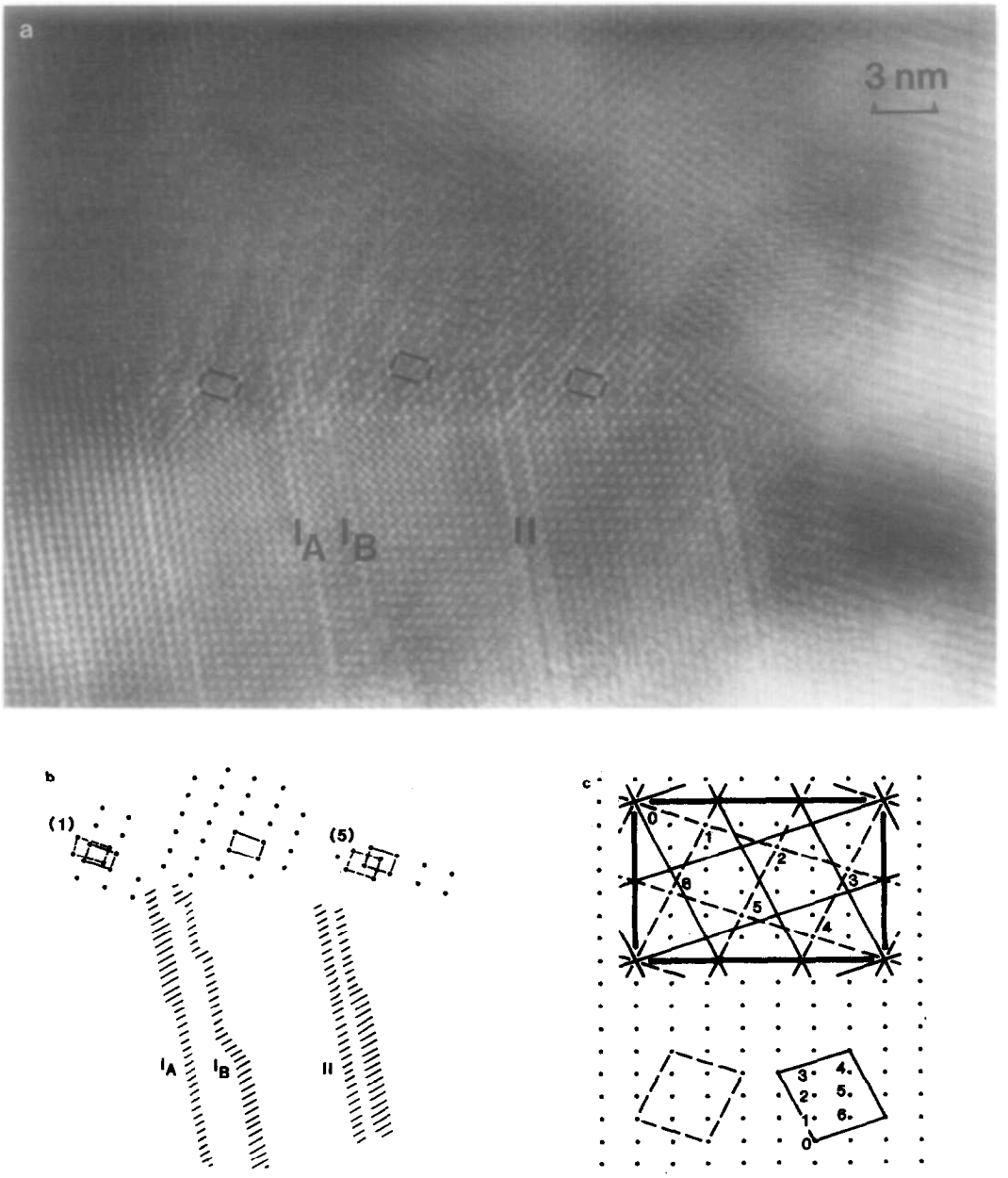

FIG. 5. (a) An electron micrograph illustrating a region of overlap of ι and ι' giving rise, in projection, to a large supercell outlined in black for three regions on the micrograph. The shift of the supercell positions relative to the substructure enables the determination of the glide vector for the I_A and I_B stacking faults. (b) A schematic drawing of the white dot superstructure in the overlap region of ι and ι'. The dotted rectangles emphasize the shift (see (5c)) of the supercells in projection that result from overlap in regions where stacking faults I and II occur. (c) The supercell in projection in the overlapping regions of ι and ι' obtained by the superposition of the images. Iota is outlined in solid lines and iota prime in dashed lines as indicated below the supercell. A shift in position of the origin of the ι structure from position 0 to 1, 2, 3, 4, 5, 6 makes, respectively, a shift in the position of the common supercell in projection from positions 0 to 6, 1, 5, 3, 4, 2. (d) A schematic representation of the stacking faults labeled I_A and I_B in (5b). Slabs of Pr_8O_{14} one unit cell wide are separated by a slab of Pr_7O_{12} three unit cells wide.

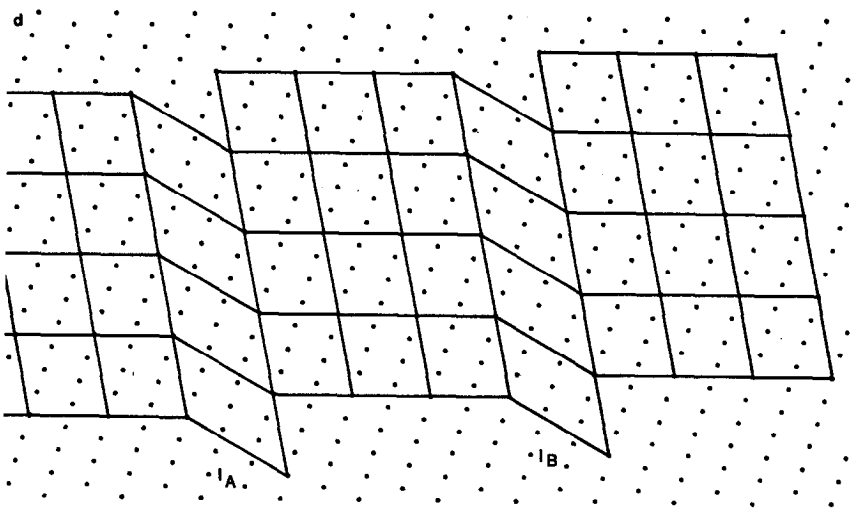

FIG. 5—*Continued.*

until they encounter one another. The experimental results fit with those expected from group theory considerations but usually only two orientation variants are seen at the same time. As indicated previously this could reflect some thin-layer effect.

From zeta. The formation of iota from zeta is very different from the previous case. Stacking faults are nearly uniquely parallel to one ⟨100⟩ direction, contrary to expectations since in the structure of iota the [100] or [010] iota directions are equivalent (valid also inside a thin-layer crystal whose surface should be close to the (001) plane of iota). The observation of the phase transition shows the origin of this phenomenon. As suggested by a previous study (*8*) iota grows in the form of needles inside zeta. Needles of iota grow so that their [100] direction is parallel to the [001] zeta direction. Why does such a well-defined orientation of iota on zeta occur while it seems not to occur if iota grows on epsilon? In contrast to epsilon, zeta has a pseudocubic cell rather far from the cubic symmetry: $a = 5.478$, $b = 5.482$, $c = 5.496$, so that a significant deformation from the cubic unit cell occurs. A nearly cubic symmetry does not occur for zeta even without taking into account the vacancies as they occur in epsilon. The result is that a seed of iota grows into a needle-like domain in a well-defined orientation relative to zeta because, as can be shown (*7, 8*), only in this way can strain-free interfaces occur. When they join, these needles give faulted regions oriented parallel to the [100] direction. If two needles growing in opposite sense encounter, a faulted region parallel to the [010] direction can occur. Such a defect can be seen in Fig. 4a.

From delta. Tb_7O_{12} obtained through $Tb_{11}O_{20}$ (delta) sometimes behaves as does Pr_7O_{12} obtained through Pr_9O_{16}. In both reactions, stacking faults corresponding to layers of different compositions occur (region A of Figs. 4 and 6). This is to be expected if the mechanism suggested above for the praseodymium oxides were to be followed here (*7*) as well. In the case of terbium, no direct observation of needles of Tb_7O_{12} inside $Tb_{11}O_{20}$ has been made but in some cases the structure of iota obtained through $Tb_{11}O_{20}$ is exactly like the structure of iota obtained through Pr_9O_{16} so that the same kind of transformation probably occurs. Nevertheless, it must be mentioned that many occurrences of Tb_7O_{12} are obtained without these characteristic stacking faults (region B of Fig. 6). It has not been

clarified whether the stacking faults disappear by annealing or by some other mechanism. Region C in Fig. 6 is an overlay of ι' and δ.

4. Orientation Variants for the Other Structures

The other structures, zeta (for praseodymium) or delta (for terbium), can easily be observed by electron microscopy in the same condition of lattice imaging (with the electron beam parallel to a $\langle 211 \rangle_F$ axis). In these cases, several variants can be observed corresponding to different possible orientations, each giving a superstructure for this orientation. Large regions without superstructure can also be seen, for example, in $Tb_{11}O_{20}$ (Fig. 7), probably corresponding to one of the four orientation variants that gives no superstructure. Stacking faults corresponding to glide domains seem to be very rare in these structures.

Conclusions

The existence of different orientation variants of R_nO_{2n-2} oxides has been shown to occur as would be expected from general point group considerations. In these theoretical predictions the R_nO_{2n-2} structures are treated as though vacancy-ordered structures were derived from a high-symmetry unordered structure of the fluorite type. The best fit with these predictions is observed when the formation of iota occurs through epsilon. When formation occurs through zeta or delta the phenomena are more complicated because of the existence

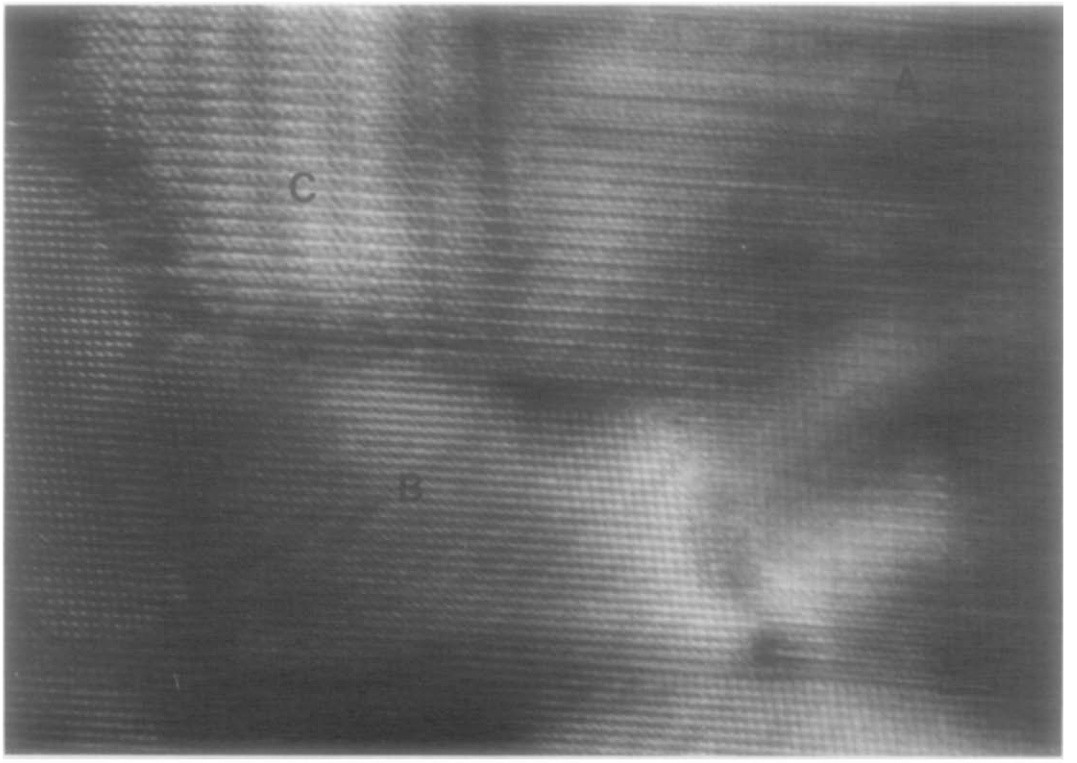

FIG. 6. An electron micrograph showing Tb_7O_{12} (iota) obtained from $Tb_{11}O_{20}$ (delta). Region A consists of layers of different composition (mainly iota and delta). Region B is iota without stacking faults or layers of a different composition. Region C is an overlay of ι' and δ.

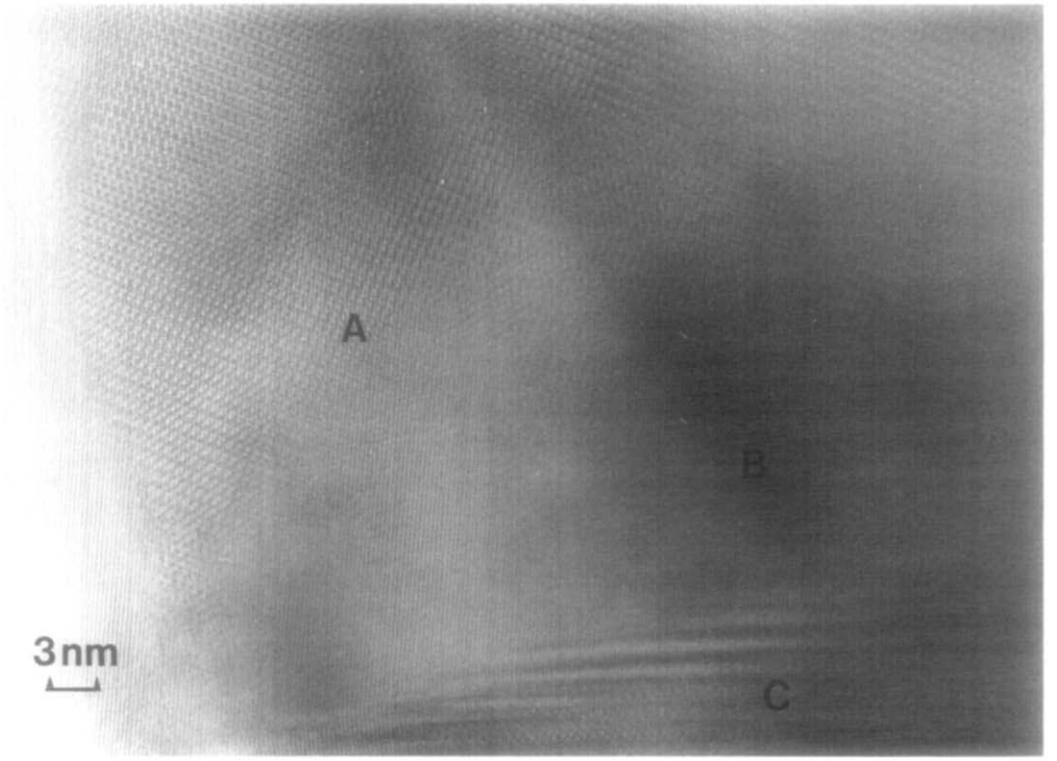

FIG. 7. An electron micrograph showing a region that is probably $Tb_{11}O_{20}$ (delta) everywhere except at the very edge of the crystal. The delta superstructure is clearly shown at A. The moiré pattern at C is caused by an overlap of two misoriented crystals of delta. Superstructure is virtually absent in region B where another orientation variant of delta with no superstructure is reasonably believed to occur. (Image taken by David Smith.)

of strain at the interface of the structures involved. The strain energy disappears by the formation of strain-free interfaces between the different structures yielding characteristic faults. Typical stacking faults in Pr_7O_{12} have been related, for example, to the formation of iota through zeta and in Tb_7O_{12} to the formation of iota through delta. These defects have been shown to be, in fact, layers of different composition. A few results have also been obtained for the zeta and delta structures.

Acknowledgment

We gratefully acknowledge NSF support through Grant DMR-8516381.

References

1. L. EYRING, *High Temp. Sci.* **20,** 183 (1985).
2. R. T. TUENGE AND L. EYRING, *J. Solid State Chem.* **41,** 75 (1982).
3. C. BOULESTEIX, P. CARO, C. LOIER, AND R. PORTIER, *Phys. Status Solidi A* **14,** 771 (1972).
4. C. BOULESTEIX, *in* "Handbook on the Physics and Chemistry of Rare Earths" (K. A. Gschneidner, Jr. and L. Eyring, Eds.), Vol. 5, Chap. 44, pp. 321–386, North-Holland, Amsterdam (1982).
5. G. VAN TENDELOO AND S. AMELINCKX, *Acta Crystallogr. Sect. A* **30,** 431 (1974).
6. J. O. SAWYER, B. G. HYDE, AND L. EYRING, *Bull. Soc. Chim. Fr.* **4,** 1190 (1965).
7. C. BOULESTEIX AND L. EYRING, to be published.
8. C. BOULESTEIX, B. YANGUI, M. BEN SALEM, C. GAUSLIKAS, AND S. AMELINCKX, *J. Phys. (Paris)* (1986).